

# Collisional loss of one-dimensional fermions near a $p$ -wave Feshbach resonance

Ya-Ting Chang,<sup>1</sup> Ruwan Senaratne,<sup>1</sup> Danyel Cavazos-Cavazos,<sup>1</sup> and Randall G. Hulet<sup>1,\*</sup>

<sup>1</sup>*Department of Physics and Astronomy, Rice University, Houston, Texas 77005, USA*

(Dated: May 27, 2022)

We study collisional loss of a quasi-one-dimensional (1D) spin-polarized Fermi gas near a  $p$ -wave Feshbach resonance in ultracold  $^6\text{Li}$  atoms. We measure the location of the  $p$ -wave resonance in quasi-1D and observe a confinement-induced shift and broadening. We find that the three-body loss coefficient  $L_3$  as a function of the quasi-1D confinement has little dependence on confinement strength. We also analyze the atom loss with a two-step cascade three-body loss model in which weakly bound dimers are formed prior to their loss arising from atom-dimer collisions. Our data are consistent with this model. We also find a possible suppression in the rate of dimer relaxation with strong quasi-1D confinement. We discuss the implications of these measurements for observing  $p$ -wave pairing in quasi-1D.

The realization of ultracold atomic Fermi gases has provided experimental access to a wide array of phenomena, largely because of the presence of Feshbach resonances that provide for externally tunable interatomic interactions [1–4]. In addition to the usual  $s$ -wave interactions between distinguishable fermions, higher partial-wave interactions may also be tuned via Feshbach resonances [5].  $p$ -Wave interactions are of particular interest as they are the dominant low-energy scattering process between identical fermions. Such systems are predicted to exhibit phenomena distinct from those observed in  $s$ -wave interacting Fermi gases [6]. In particular, pairing between identical fermions is an essential ingredient of the Kitaev chain Hamiltonian [7], which supports Majorana zero-modes at the ends of the chain. These zero-modes have been observed in semiconducting nanowires [8], and are a promising candidate platform for fault-tolerant quantum computing [9, 10].

$p$ -Wave Feshbach resonances have been observed in  $^{40}\text{K}$  [11–13] and  $^6\text{Li}$  [14–19]. The severe atom losses associated with these resonances, however, have limited their usefulness. Three-body losses, which are suppressed by symmetry in the case of a fermionic two-spin system with  $s$ -wave interactions [20], are not suppressed, and are consequently significant for  $p$ -wave interactions. Much work has been done recently in characterizing the atom loss associated with  $p$ -wave Feshbach resonances [21–24], and there has been renewed interest in studying these resonances in reduced dimensions. Recent theoretical work has suggested that three-body losses may be suppressed in the quasi-1D traps that are achievable in ultracold atom experiments [25]. The absence of a centrifugal barrier in 1D results in Feshbach molecules that have extended wavefunctions which overlap less with deeply-bound molecular states. This may result in suppressed three-body loss,

and if confirmed might open a path towards realizing  $p$ -wave pairing in quasi-1D and emulating the Kitaev chain Hamiltonian.

In this paper, we present an experimental study of three-body losses near a  $p$ -wave Feshbach resonance of identical  $^6\text{Li}$  fermions in quasi-1D. We measure the three-body loss coefficient ( $L_3$ ) as a function of 1D confinement for a direct three-body process, and observe no dependence up to our maximum confinement strength. We also analyze the observed atom loss within the framework of a cascade model, in which a transient Feshbach dimer formed in an initial atom-atom collision is subsequently lost due to the formation of a deeply-bound molecule in an inelastic atom-dimer collision [26, 27]. We find that the atom-dimer collision rate is nearly independent of magnetic field for large field detunings from resonance, but the data suggest a possible suppression for fields closer to resonance. Finally, we characterize the confinement-induced shifts in the resonance position that appear in quasi-1D [28–32]. These shifts allow us to extract a value for the effective range that is in agreement with our coupled-channel calculations, as well as our new analysis of previous experimental work in quasi-2D [21].

The apparatus and the experimental methods we use to prepare degenerate Fermi gases have been described previously [33, 34]. A  $^6\text{Li}$  degenerate Fermi gas is first prepared in the two lowest hyperfine states of the  $S_{1/2}$  manifold (states  $|1\rangle$  and  $|2\rangle$ , respectively) at 595 G, corresponding to an  $s$ -wave scattering length of  $326 a_0$ , where  $a_0$  is the Bohr radius. The atoms are then loaded into a crossed-beam dipole trap formed by three linearly-polarized mutually-orthogonal laser beams of wavelength  $\lambda = 1.064 \mu\text{m}$ . Each beam is retro-reflected, with the polarizations of the incoming and retro-reflected beams set to be perpendicular to each other to avoid lattice

formation. We then eliminate state  $|1\rangle$  from the trap with a resonant burst of light. At this stage, we obtain  $9(1) \times 10^4$  atoms in state  $|2\rangle$  in a nearly isotropic harmonic trap with a geometric-mean trapping frequency of  $2\pi \times 305(2)$  Hz, and at a temperature  $T/T_F \approx 0.1$  where,  $T_F$  is the Fermi temperature. The optical trap depths are increased and the polarizations of the retro-reflected beams are rotated to achieve a  $7 E_r$  deep 3D optical lattice, where  $E_r = \hbar^2/(2m\lambda^2) = k_B \times 1.41 \mu\text{K}$  is the recoil energy, and  $m$  is the atomic mass. During the lattice ramp, a co-propagating (but not retro-reflected) beam of blue-detuned light (532 nm) is introduced along each trapping-beam dimension to reduce the curvature of the trapping potential [33, 34]. By tuning these compensation beam powers, we create a 3D band insulator with a central density of approximately 1 atom per site at the center of the cloud. In order to produce a 2D lattice, which is an array of quasi-1D tubes, we slowly turn off the compensation beams and the vertical lattice beam, while increasing the intensity of the two remaining beams to achieve a desired 2D lattice depth,  $V_L$ . The final 2D lattice depth determines the confinement in the quasi-1D traps, which is parameterized by  $a_\perp = \sqrt{\hbar/m\omega_r}$  and  $R_F$ , where  $\omega_r = \sqrt{4E_r V_L}/\hbar$  is the trapping frequency of a lattice site when approximated as a harmonic potential, and  $R_F(N_{t,j}, \omega_z) = \sqrt{(2N_{t,j} + 1)\hbar/m\omega_z}$  is the Fermi radius of tube  $j$  with number of atoms  $N_{t,j}$  and an axial frequency  $\omega_z$ . The aspect ratio of the quasi-1D tubes  $\Lambda = \omega_r/\omega_z$  is independent of lattice depth, and is approximately 165. We load a maximum of around 30 atoms per quasi-1D tube with a temperature below the Fermi temperature to avoid exciting any radial modes.

Because the  ${}^6\text{Li}$   $|1\rangle - |1\rangle$   $p$ -wave Feshbach resonance near 159 G is very narrow in magnetic field, we use a two-step servo scheme to stabilize the current in the coils producing the Feshbach magnetic field. The first servo,  $S_1$ , provides the large dynamic range required to run our experimental sequence, while the second servo,  $S_2$ , controls the current in a bypass circuit added in parallel to the magnetic coils. This improves the stability of the magnetic field to  $\pm 10$  mG and provides finer magnetic-field resolution. After reaching the hold field  $B$ , the atoms are transferred into  $|1\rangle$  with a  $\pi$ -pulse of duration  $75 \mu\text{s}$  using RF radiation resonant with the  $|1\rangle - |2\rangle$  magnetic-dipole transition, where they interact via the  $p$ -wave Feshbach resonance. After a hold time  $\tau$ , we ramp the field back to 595 G to take an image of the atoms.

We image the remaining atoms with one of two possible imaging techniques, absorption imaging after the cloud undergoes free expansion, or *in situ* phase-contrast

imaging. The former technique is state-selective, but does not provide information on the typically non-uniform distribution of atoms across the array of quasi-1D tubes. The latter technique, when coupled with the inverse Abel transform, which exploits the approximate cylindrical symmetry of the 2D lattice, enables us to measure this distribution with a resolution of approximately three lattice constants. We use the measured density distribution to sector the 2D lattice into concentric shells in which the tubes have similar chemical potentials, as shown in Fig. 1. This procedure is useful as scattering processes are in general energy-dependent, so observables depend on rate coefficients that are averaged over the Fermi-Dirac distribution for atoms in each tube.

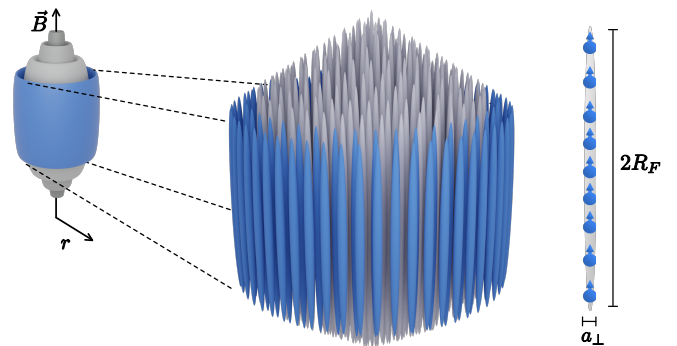


FIG. 1. Schematic representing the multiple cylindrical shells that can be accessed through *in situ* imaging. A particular shell  $i$  composed of multiple tubes  $j$  is highlighted in blue. A homogeneous magnetic field is applied along the axial ( $z$ ) direction. Because of the magnetic field alignment, only the  $|m_l| = 0$  projection of the angular momentum in the  $p$ -wave collisions is allowed. Each tube is characterized axially by a 1D Fermi radius  $R_F$ , and transversely by the harmonic oscillator length scale  $a_\perp$ .

We characterized the  $|1\rangle - |1\rangle$   $p$ -wave Feshbach resonance in 3D and quasi-1D, by measuring atom loss as functions of  $B$  and  $\tau$ . In the same 3D trap that we prepare the ultracold atoms, we find the onset of loss at  $B_{3D} = 159.05(1)$  G, which agrees with the previous measurements of the location of this resonance in 3D [15, 17] but differs with other measurements [19, 35] by a few 10's of mG. We were not able to resolve the expected doublet feature arising from the dipole-dipole interaction [12, 19, 36] because of limitations of the field stability. As  $V_L$  is increased, we observe a confinement-induced shift in the resonance field and broadening of the atom-loss feature, as shown in Fig. 2(a).

We now review  $p$ -wave scattering in 3D and quasi-1D

to show how the measured confinement-induced shift can be used to extract  $\alpha_p$ , the 3D effective range. For low-energy collisions in 3D, the cotangent of the phase-shift  $\delta_p$  associated with  $p$ -wave scattering can be expanded as a function of two parameters, the  $p$ -wave scattering volume,  $V_p$ , and a  $p$ -wave effective range,  $\alpha_p$  [37]:

$$k^3 \cot(\delta_p(k)) = -\frac{1}{V_p} - \alpha_p k^2 + O(k^4). \quad (1)$$

The effective range is positive and has units of inverse length, unlike in the case of  $s$ -wave scattering, where it has units of length. Both the scattering volume and the effective range may be obtained as a function of magnetic field by solving the Schrödinger equation for the relevant coupled-channel system at low energy. These scattering properties are modified in quasi-1D,

$$k \cot(\delta_p(k)) = -\frac{1}{l_p} - \xi_p k^2 + O(k^4), \quad (2)$$

where  $l_p$  is the 1D  $p$ -wave scattering length and  $\xi_p$  is the 1D  $p$ -wave effective range, which has units of length. These quasi-1D scattering parameters are given by [30–32]:

$$l_p = 3a_\perp \left[ \frac{a_\perp^3}{V_p} + \alpha_p a_\perp + 3\sqrt{2}|\zeta(-1/2)| \right]^{-1} \quad (3)$$

and

$$\xi_p = \alpha_p a_\perp^2 / 3, \quad (4)$$

where  $\zeta$  is the Riemann zeta function ( $\zeta(-1/2) \approx -0.208$ ). The second and third terms in  $l_p$  lead to a confinement-induced shift in the resonance location.

By performing a coupled-channel calculation, which requires detailed knowledge of the inter-atomic potentials [38], we obtain an expansion  $1/V_p(B)$  up to second order in  $B$ . The effective range  $\alpha_p$  can be approximated as a constant independent of  $B$  for the relevant range of magnetic field. The Feshbach resonance in 3D occurs at the magnetic field  $B_{3D}$  at which  $V_p$  diverges. Similarly, in quasi-1D, the resonance occurs when  $l_p$  diverges at a magnetic field  $B_{1D}$ , which is a function of  $V_L$  and  $\alpha_p$ . The confinement-induced shift,  $\delta_B(V_L, \alpha_p) = B_{1D} - B_{3D}$ , can be approximated to leading order in confinement strength by (see Supplemental Material [39])

$$\delta_B = \frac{-2mE_r}{\hbar^2 \frac{\partial(1/V_p)}{\partial B}|_{B=B_{3D}}} \alpha_p \sqrt{V_L}. \quad (5)$$

We fit the measured confinement-induced shifts as a function of  $V_L$  to Eq. 5 by taking  $\alpha_p$  and  $B_{3D}$  as fitting parameters. The result of the fit to the quasi-1D data is shown by the solid curve in Fig. 2(b). We obtain an effective range  $\alpha_p = 0.14(1) a_0^{-1}$ . We find a consistent value by analyzing previous measurements performed on a 2D gas of  ${}^6\text{Li}$  in state  $|1\rangle$  [21] (see Supplemental Material [39]). The measured  $\alpha_p$  is also consistent with our coupled-channel result of  $0.1412 a_0^{-1}$ .

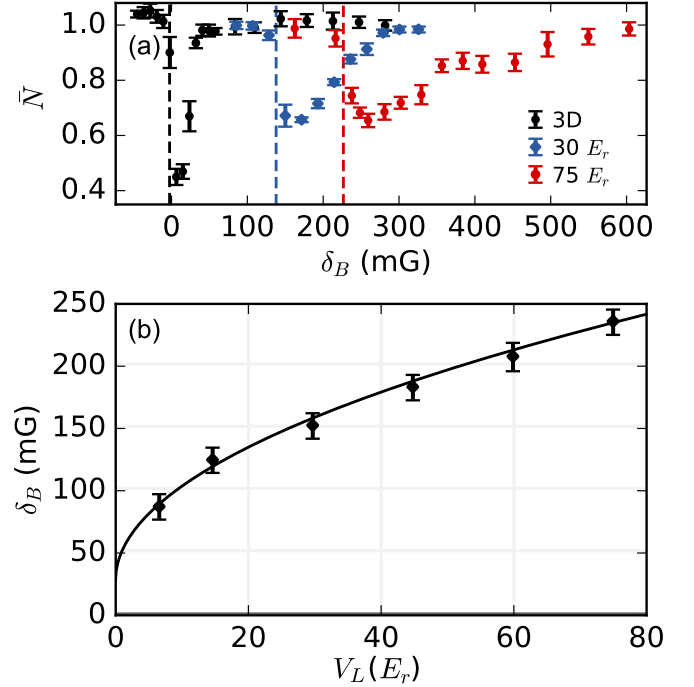


FIG. 2. (a)  $p$ -Wave resonances in 3D and quasi-1D measured with magnetic-field-dependent loss. We define  $\delta_B(V_L, \alpha_p) = B_{1D} - B_{3D}$ , where we measure  $B_{3D} = 159.05(1)$  G. The resonance position for each case (dashed line) corresponds to the onset (15% loss) of the observed atomic loss averaged over 6 experimental runs. Error bars are the standard error of the mean. (b) The diamonds show the confinement-induced shift,  $\delta_B$ , for the quasi-1D  $p$ -wave Feshbach resonance position as a function of  $V_L$ . The solid curve shows the result of fitting the data to Eq. 5, where the effective range  $\alpha_p = 0.14(1) a_0^{-1}$  and  $B_{3D} = 159.07(1)$  G are fitted parameters. Error bars indicate the statistical uncertainty arising from atom number fluctuation and field instability.

The observed atom loss is presumably due to the formation of deeply-bound molecules. To characterize the observed loss, we measured  $N$ , the number of atoms remaining in the trap after a holdtime  $\tau$  for various  $B$  and  $V_L$ . Background-gas collisions lead to a  $1/e$  atom lifetime

of 38 s in this apparatus, and are negligible for this analysis. Atom loss due to three-body collisions is described by

$$\frac{\dot{N}}{N} = -L_3 n^2, \quad (6)$$

where  $n^2 = (N_{t,c}/2R_{F,c})^2$  is the squared atomic line density for a central tube, determined using a length-scale of twice the local Fermi radius  $R_{F,c}$ . We measure the time evolution with  $V_L$  between 15 to 75  $E_r$  and extract  $L_3$  by fitting loss vs time to Eq. 6. The peak three-body loss coefficients for all measured lattice depths in the range of 15  $E_r$  to 75  $E_r$  are around  $7(2) \times 10^{-6}$  cm<sup>2</sup>/s. We observe no dependence on 1D confinement in this range. Due to the inhomogeneity of the initial distribution of atoms across the 2D lattice, however, we find a rather poor agreement of the data to Eq. 6 (see Supplemental Material [39]).

An alternative analysis of the same data that provides an improved fit is shown in Fig. 3. Here, we group the tubes into separate cylindrical shells (labeled by  $i = 1 - 4$ ) with an averaged atom number per tube  $\langle N_t \rangle_i$  and a corresponding Fermi temperature  $T_{F,i}$ . Figure 4(a) shows

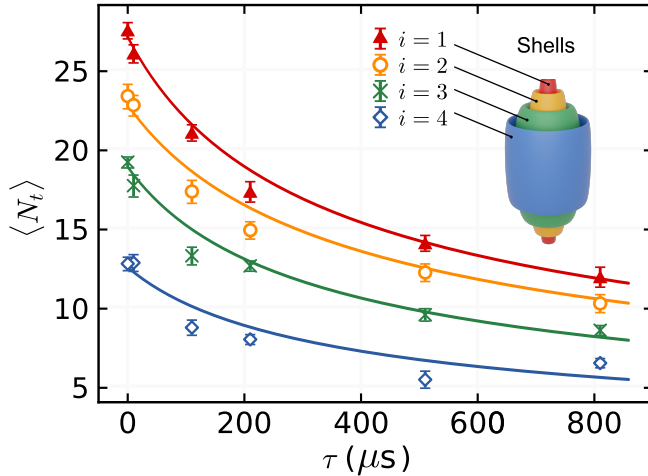


FIG. 3. Typical time evolution of averaged tube population  $\langle N_t \rangle$  in 4 shells at  $\Delta B = 30$  mG with  $V_L = 75 E_r$ . The different colors and symbols indicate different shells with approximately uniform initial atom number per tube. The shells are labeled from  $i = 1$ , the inner-most, to  $i = 4$ , the outer-most shell. Solid curves show fits to Eq. 6 to extract  $L_3$  with the squared atomic density  $n^2 = (\langle N_t \rangle_i / 2R_{F,i})^2$  of a typical tube in each shell, and the corresponding Fermi radii. The corresponding  $L_3$  values are plotted in Fig. 4. Data points are averaged over 5 shots, and error bars are the standard error of the mean.

$L_3$  for each shell extracted from this data. The peak  $L_3$  for each shell is in the range of  $5 \times 10^{-6}$  cm<sup>2</sup>/s to  $1 \times 10^{-5}$  cm<sup>2</sup>/s, and is similar to the peak  $L_3$  extracted from the whole atomic cloud.

Recently, the loss of ultracold fermions near a  $p$ -wave Feshbach resonance in 3D has been modeled as a cascade of two consecutive two-body processes. Two atoms resonantly form a Feshbach dimer, followed by a collision between the dimer and an atom, and result in a deeply-bound molecule and an atom [26, 27]. The differential equations governing this loss process are

$$\frac{dN_a}{dt} = 2\frac{\Gamma}{\hbar}N_d - 2K_{aa}\frac{N_a(N_a-1)}{4R_F} - K_{ad}\frac{N_aN_d}{2R_F} \quad (7)$$

and

$$\frac{dN_d}{dt} = -\frac{\Gamma}{\hbar}N_d + K_{aa}\frac{N_a(N_a-1)}{4R_F} - K_{ad}\frac{N_aN_d}{2R_F}, \quad (8)$$

where  $N_a$  is the number of atoms,  $N_d$  is the number of Feshbach dimers,  $K_{aa}$  is the two-body event rate for atom-atom collisions converting atoms into Feshbach dimers, and  $K_{ad}$  is the two-body atom-dimer inelastic collision event rate. The decay rate of dimers is determined by the width of the Feshbach resonance,  $\Gamma$ . The rate of dimer formation is proportional to the number of possible pairs of atoms, given by  $N_a(N_a-1)/2!$  and typically approximated as  $N_a^2/2$  for large  $N_a$ . However, in our experiment, the atom number per quasi-1D tube is quite small ( $\approx 30$ ), and thus we use the exact form in our analysis.

Both  $\Gamma$  and  $K_{aa}$  are related to the elastic scattering cross-section,  $\sigma_{1D}(E)$ , which can be calculated, thus constraining the fit to the cascade process by a single fitting parameter,  $K_{ad}$ . The elastic scattering cross-section may be approximated by a Lorentzian in terms of the collision energy,  $E = \hbar^2 k^2 / m$  as follows (see Supplemental Material [39]):

$$\sigma_{1D}(E) \approx \frac{(\frac{\Gamma}{2})^2}{(E - E_{\text{res}})^2 + (\frac{\Gamma}{2})^2}. \quad (9)$$

Here,  $E_{\text{res}} = -\hbar^2 / l_p \xi_p m > 0$  for  $l_p < 0$  is the above-threshold binding energy of the Feshbach molecule, and  $\Gamma = (\hbar / \xi_p) \sqrt{4E_{\text{res}} / m}$  is the width of the resonance [6].

The scattering cross-section may be used to calculate  $K_{aa}$ , which is the average of  $\sigma_{1D}(k_r)$  over the ensemble of pairs of atoms with relative momentum  $k_r$  and velocity  $v_r$

$$K_{aa} = \langle \sigma_{1D}(k_r) v_r \rangle = \hbar \int_{-\infty}^{\infty} dk_r \sigma_{1D}(k_r) v_r P(k_r), \quad (10)$$

and

$$P(k_r) = \frac{\hbar}{N_a^2} \int_{-\infty}^{\infty} dk' n(k') n(k' - k_r). \quad (11)$$

The  $k$ -space number density is given by

$$n(k) = \frac{1}{2\pi\hbar} \int_{-\infty}^{\infty} dx \frac{1}{\exp[\beta(\frac{1}{2}m\omega_z^2 x^2 + \frac{\hbar^2 k^2}{2m} - \mu)] + 1}, \quad (12)$$

where  $\beta = 1/k_B T$  and  $\mu$  is the chemical potential. We assume a global temperature across the entire sample. However, the chemical potential varies significantly from tube-to-tube due to the density inhomogeneity across the 2D lattice. This effect is mitigated by sectoring the cloud into shells of similar chemical potential, as discussed earlier, and calculating a distinct value of  $K_{aa}$  for each shell. For each quasi-1D tube,  $\mu$  is determined (through normalizing Eq. 12) by the atom number in that tube and the temperature. We determined the average atom number per tube for each shell by performing the inverse Abel transform.

Although we cannot directly measure  $T$ , we exploit the fact that at a sufficiently large magnetic field detuning  $\Delta B = B - B_{1D}$ , where  $B_{1D}$  is the magnetic field at the Feshbach resonance for a particular  $V_L$ , the rate equations can be approximated by a three-body loss equation with  $L_3 = (3/2!) \hbar K_{ad} K_{aa} / \Gamma$  [27]. By comparing  $\hbar K_{aa} / \Gamma$  to our measured values of  $L_3$  for  $\Delta B > 100$  mG, as shown in Fig. 4(a), we determine  $T = 0.1 T_{F,1}$ , and by carrying out the integrations in Eqs. 10-12 numerically, we obtain  $K_{aa}$  for each shell.

The extracted atom-dimer collision event rate  $K_{ad}$  for  $V_L = 75 E_r$  is shown in Fig. 4(b). The relative uniformity of  $K_{ad}$  for  $\Delta B > 50$  mG is evidence that the cascade model is appropriate and conforms to a previous analysis of 3D and quasi-2D measurements on the same Feshbach resonance [27]. The large uncertainty in the fitted value for the outermost shell is indicative of its small  $N_t$ .

The behavior of  $K_{ad}$  for  $\Delta B < 50$  mG could be a consequence of the suppression predicted by Zhou and Cui [25]. In quasi-1D the predicted suppression of dimer relaxation would manifest as a suppression of  $K_{ad}$ . The stretching of the quasi-1D  $p$ -wave molecule wavefunction is expected to be significant for  $\sqrt{2}\kappa a_{\perp} < 1/2$ , where  $\kappa = \sqrt{mE_{\text{res}}}/\hbar$  [25]. This suppression is predicted to be strongest for small  $\Delta B$ , where the binding energy of the Feshbach molecule,  $E_{\text{res}}$ , is smallest. For  $V_L = 75 E_r$ , this condition corresponds to  $\Delta B < 27$  mG. The suppression we observe is relatively mild (around a factor of 2), however, and only relevant in a narrow magnetic field range

near the resonance, limiting its experimental usefulness. Another interpretation of the small-detuning behavior of  $K_{ad}$  is that the cascade model breaks down and is no longer applicable, perhaps due to unitarity effects [24], or due to the existence of a shallow three-body bound state as recently suggested by Schmidt *et al.* [40].

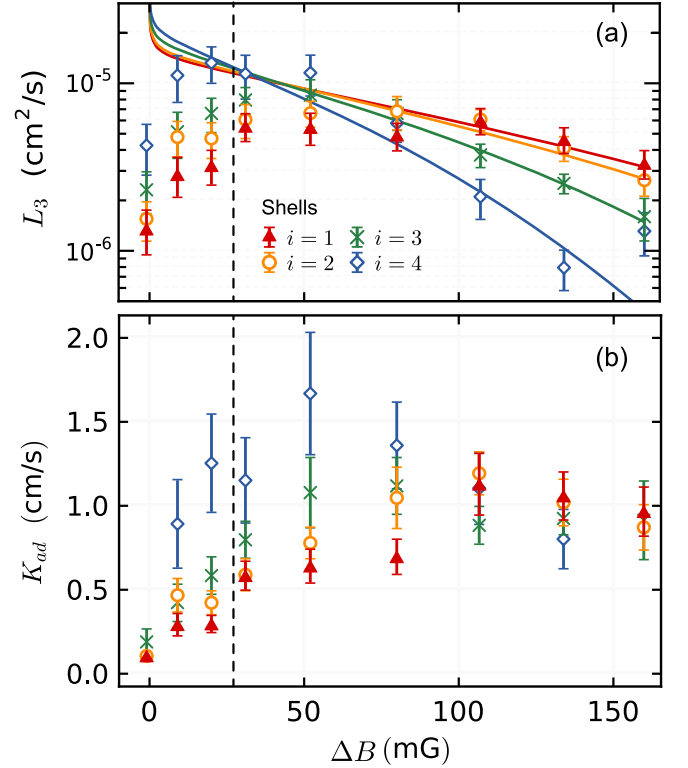


FIG. 4. (a)  $L_3$  as a function of magnetic field detuning  $\Delta B$  for  $V_L = 75 E_r$ .  $L_3$  is extracted from fitting  $N_{t,i}$  for each shell vs  $\tau$  with Eq. 6, as shown for  $\Delta B = 30$  in Fig 3. Solid curves show  $(3/2!) \hbar K_{ad} K_{aa} / \Gamma$  with a constant  $3K_{ad}/2! = 1$  cm/s, calculated for  $T = 0.1 T_{F,1}$ . (b) Atom-dimer collision event rate  $K_{ad}$  as a function of magnetic field detuning  $\Delta B$ .  $K_{ad}$  is extracted by fitting  $\langle N_t \rangle_i$  vs  $\tau$  to Eqs. 7 and 8, using the calculated values of  $\Gamma$  and  $K_{aa}$ . The black dashed line indicates  $\Delta B = 27$  mG, which corresponds to  $\sqrt{2}\kappa a_{\perp} = 1/2$  for  $V_L = 75 E_r$  [25]. Error bars indicate the one-sigma confidence interval for the fitting parameters  $L_3$  and  $K_{ad}$ , respectively.

This work is the first detailed experimental study of  $p$ -wave collisions in quasi-1D. We confirm the confinement-induced shift and broadening as a function of lattice depth  $V_L$ . The confinement-induced shift agrees well with quasi-1D theory [32] and the extracted value for the 3D effective range  $\alpha_p$  agrees with previous work [21]. We measure the three-body loss coefficient  $L_3$  as a function of  $V_L$  and find

no dependence up to  $75 E_r$ . The magnetic field independence of  $K_{ad}$  for  $\Delta B > 50$  mG confirms the cascade model [26, 27] for three-body loss in quasi-1D in the regime of large magnetic field detuning, as well as for intermediate magnetic field detunings where the loss cannot be approximated by the three-body loss equation. The suppression in  $K_{ad}$  at  $\Delta B < 50$  mG is possibly explained by  $p$ -wave molecule stretching [25]. Achieving greater suppression by increasing  $V_L$  would be challenging since at a fixed magnetic field detuning  $\Delta B$ ,  $\kappa$  is independent of  $V_L$ , and thus  $\kappa a_{\perp} \propto 1/V_L^{1/4}$  (see Supplemental Material [39]).

Although we do not have clear evidence of a suppression of atom loss, future work at even higher lattice depths could be fruitful as the increased confinement should expand the magnetic field range over which the molecular wavefunction is extended. Similarly, improved magnetic field resolution and stability would enable further study of this narrow feature closer to resonance. These technical advancements could improve the prospects of detecting  $p$ -wave pairing and emulating the Kitaev chain Hamiltonian.

We would like to thank T. L. Yang for his contributions to the apparatus and W. I. McAlexander for his coupled-channel code. This work was supported in part by the Army Research Office Multidisciplinary University Research Initiative (Grant Nos. W911NF-14-1-0003 and W911NF-17-1-0323), the NSF (Grant No. PHY-1707992), and the Welch Foundation (Grant No. C-1133). D. C. acknowledges financial support from CONACyT (Mexico, Scholarship No. 472271).

---

\* randy@rice.edu

- [1] B. DeMarco and D. S. Jin, *Science* **285**, 1703 (1999).
- [2] A. G. Truscott, K. E. Strecker, W. I. McAlexander, G. B. Partridge, and R. G. Hulet, *Science* **291**, 2570 (2001).
- [3] F. Schreck, L. Khaykovich, K. L. Corwin, G. Ferrari, T. Bourdel, J. Cubizolles, and C. Salomon, *Phys. Rev. Lett.* **87**, 080403 (2001).
- [4] S. R. Granade, M. E. Gehm, K. M. O'Hara, and J. E. Thomas, *Phys. Rev. Lett.* **88**, 120405 (2002).
- [5] C. Chin, R. Grimm, P. Julienne, and E. Tiesinga, *Rev. Mod. Phys.* **82**, 1225 (2010).
- [6] V. Gurarie and L. Radzihovsky, *Ann. Phys. (NY)* **322**, 2 (2007).
- [7] A. Y. Kitaev, *Phys. Usp.* **44**, 131 (2000).
- [8] S. D. Sarma, M. Freedman, and C. Nayak, *Quantum Inf.* **1**, 15001 (2015).
- [9] S. B. Bravyi and A. Y. Kitaev, *Ann. Phys. (NY)* **298**, 210 (2002).
- [10] A. Stern and N. H. Lindner, *Science* **339**, 1179 (2013).
- [11] C. A. Regal, C. Ticknor, J. L. Bohn, and D. S. Jin, *Phys. Rev. Lett.* **90**, 053201 (2003).
- [12] K. Günter, T. Stöferle, H. Moritz, M. Köhl, and T. Esslinger, *Phys. Rev. Lett.* **95**, 230401 (2005).
- [13] C. Luciuk, S. Trotzky, S. Smale, Z. Yu, S. Zhang, and J. H. Thywissen, *Nat. Phys.* **12**, 599 (2016).
- [14] J. Zhang, E. G. M. van Kempen, T. Bourdel, L. Khaykovich, J. Cubizolles, F. Chevy, M. Teichmann, L. Tarruell, S. J. J. M. F. Kokkelmans, and C. Salomon, *Phys. Rev. A* **70**, 030702 (2004).
- [15] C. H. Schunck, M. W. Zwierlein, C. A. Stan, S. M. F. Raupach, W. Ketterle, A. Simoni, E. Tiesinga, C. J. Williams, and P. S. Julienne, *Phys. Rev. A* **71**, 045601 (2005).
- [16] Y. Inada, M. Horikoshi, S. Nakajima, M. Kuwata-Gonokami, M. Ueda, and T. Mukaiyama, *Phys. Rev. Lett.* **101**, 100401 (2008).
- [17] J. Fuchs, C. Ticknor, P. Dyke, G. Veeravalli, E. Kuhnle, W. Rowlands, P. Hannaford, and C. J. Vale, *Phys. Rev. A* **77**, 053616 (2008).
- [18] R. A. W. Maier, C. Marzok, C. Zimmermann, and P. W. Courteille, *Phys. Rev. A* **81**, 064701 (2010).
- [19] M. Gerken, B. Tran, S. Häfner, E. Tiemann, B. Zhu, and M. Weidemüller, *Phys. Rev. A* **100**, 050701 (2019).
- [20] D. S. Petrov, C. Salomon, and G. V. Shlyapnikov, *Phys. Rev. Lett.* **93**, 090404 (2004).
- [21] M. Waseem, Z. Zhang, J. Yoshida, K. Hattori, T. Saito, and T. Mukaiyama, *J. Phys. B* **49**, 204001 (2016).
- [22] M. Waseem, T. Saito, J. Yoshida, and T. Mukaiyama, *Phys. Rev. A* **96**, 062704 (2017).
- [23] J. Yoshida, T. Saito, M. Waseem, K. Hattori, and T. Mukaiyama, *Phys. Rev. Lett.* **120**, 133401 (2018).
- [24] M. Waseem, J. Yoshida, T. Saito, and T. Mukaiyama, *Phys. Rev. A* **98**, 020702 (2018).
- [25] L. Zhou and X. Cui, *Phys. Rev. A* **96**, 30701 (2017).
- [26] J. Li, J. Liu, L. Luo, and B. Gao, *Phys. Rev. Lett.* **120**, 193402 (2018).
- [27] M. Waseem, J. Yoshida, T. Saito, and T. Mukaiyama, *Phys. Rev. A* **99**, 052704 (2019).
- [28] M. Olshanii, *Phys. Rev. Lett.* **81**, 938 (1998).
- [29] T. Bergeman, M. G. Moore, and M. Olshanii, *Phys. Rev. Lett.* **91**, 163201 (2003).
- [30] B. E. Granger and D. Blume, *Phys. Rev. Lett.* **92**, 133202 (2004).
- [31] L. Pricoupenko, *Phys. Rev. Lett.* **100**, 170404 (2008).
- [32] D. V. Kurlov and G. V. Shlyapnikov, *Phys. Rev. A* **95**, 032710 (2017).
- [33] R. A. Hart, P. M. Duarte, T.-L. Yang, X. Liu, T. Paiva, E. Khatami, R. T. Scalettar, N. Trivedi, D. A. Huse, and R. G. Hulet, *Nature* **519**, 211 (2015).
- [34] T. L. Yang, P. Grišins, Y. T. Chang, Z. H. Zhao, C. Y. Shih, T. Giamarchi, and R. G. Hulet, *Phys. Rev. Lett.* **121**, 103001 (2018).
- [35] T. Nakasuji, J. Yoshida, and T. Mukaiyama, *Phys. Rev. A* **88**, 12710 (2013).
- [36] C. Ticknor, C. A. Regal, D. S. Jin, and J. L. Bohn, *Phys. Rev. A* **69**, 042712 (2004).

- [37] C. J. Joachain, *Quantum Collision Theory* (North-Holland, 1975).
- [38] M. Houbiers, H. T. C. Stoof, W. I. McAlexander, and R. G. Hulet, Phys. Rev. A **57**, R1497 (1998).
- [39] See Supplemental Material at [URL] for information regarding the derivation of Eq. 5, the confinement induced shift in quasi-2D, the dependence of  $L_3$  vs  $V_L$ , the quasi-1D  $p$ -wave scattering cross-section, and the dependence of  $\kappa a_\perp$  on  $V_L$ .
- [40] M. Schmidt, H.-W. Hammer, and L. Platter, Phys. Rev. A **101**, 062702 (2020).

## Supplementary material for “Collisional loss of one-dimensional fermions near a $p$ -wave Feshbach resonance”

Ya-Ting Chang, Ruwan Senaratne, Danyel Cavazos-Cavazos, and Randall G. Hulet\*

*Department of Physics and Astronomy, Rice University, Houston, Texas 77005, USA*

(Dated: May 27, 2022)

### CONFINEMENT-INDUCED SHIFT $\delta_B$ IN QUASI-1D

The Feshbach resonance occurs at a magnetic field  $B_{1D}$  where the 1D  $p$ -wave scattering length  $l_p$  diverges [1–3]

$$\frac{1}{l_p} = \frac{a_{\perp}^3}{V_p} + \alpha_p a_{\perp} + 3\sqrt{2}|\zeta(-1/2)| = 0. \quad (\text{S1})$$

Since  $\alpha_p a_{\perp} \gg 3\sqrt{2}|\zeta(-1/2)|$  for the lattice depths  $V_L$  we can achieve in this experiment, Eq. S1 can be approximated using  $1/V_p = -\alpha_p/a_{\perp}^2$ . By Taylor expanding this around the 3D resonance field  $B_{3D}$  to first order

$$\frac{1}{V_p}|_{B=B_{1D}} = \frac{1}{V_p}|_{B=B_{3D}} + \frac{\partial(1/V_p)}{\partial B}|_{B=B_{3D}}(B_{1D} - B_{3D}) = -\frac{\alpha_p}{a_{\perp}^2}, \quad (\text{S2})$$

we obtain a simple analytical form for the confinement-induced shift  $\delta_B(V_L, \alpha_p) = B_{1D} - B_{3D}$

$$\begin{aligned} \delta_B &= \frac{-\alpha_p}{\frac{\partial(1/V_p)}{\partial B}|_{B=B_{3D}} a_{\perp}^2} \\ &= \frac{-2mE_r}{\hbar^2 \frac{\partial(1/V_p)}{\partial B}|_{B=B_{3D}}} \alpha_p \sqrt{V_L}, \end{aligned} \quad (\text{S3})$$

where  $\frac{\partial(1/V_p)}{\partial B}|_{B=B_{3D}} < 0$ .

### CONFINEMENT-INDUCED SHIFT $\delta_{B,2D}$ IN QUASI-2D

Similar to the confinement-induced shift in quasi-1D, an equivalent expression to Eq. S3 can be derived for this geometry by considering the quasi-2D scattering parameters [3]. The confinement-induced shift in quasi-2D  $\delta_{B,2D} = B_{2D} - B_{3D}$  can be approximated by

$$\delta_{B,2D} = \frac{1}{2} \delta_B. \quad (\text{S4})$$

The open circles in Fig. S1 shows the data of  $\delta_B$  in quasi-2D from [4], and the solid curve shows the result of a fit to Eq. S4 with the effective range  $\alpha_p = 0.158(5) a_0^{-1}$  as a fitting parameter. This value of  $\alpha_p$  is within 15% of the value the authors of [4] obtained by fitting measurements of the dissociation energy, as well as the value extracted from the fit to our quasi-1D data shown in the main text.

---

\* randy@rice.edu

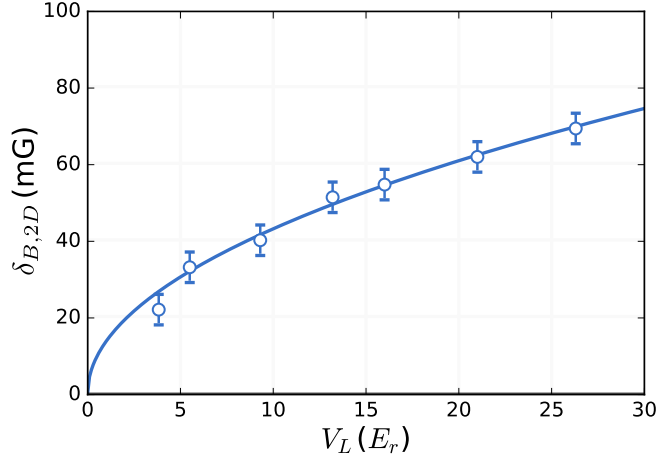


Figure S1. The open circles show the confinement-induced shift for the quasi-2D  $p$ -wave Feshbach resonance position as a function of the corresponding lattice depth (data from [4]). The solid curve shows the result of fit to Eq. S4, with the effective range  $\alpha_p = 0.158(5) a_0^{-1}$ .

### THREE-BODY LOSS COEFFICIENT $L_3$ VERSUS $V_L$

Atom loss due to three-body collisions is governed by

$$\frac{\dot{N}}{N} = -L_3 n^2. \quad (\text{S5})$$

The three-body loss coefficient  $L_3$  is obtained by fitting the time evolution of the total number of atoms  $N$  to Eq. S5, where  $n^2 = (N_{t,c}/2R_{F,c})^2$  is the squared atomic line density for a central tube, with a volume of twice the local Fermi radius  $R_{F,c}$ . A typical time evolution and fit to Eq. S5 is shown in Fig. S2.

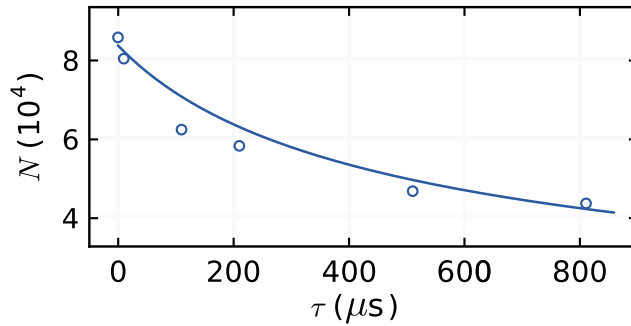


Figure S2. Typical time evolution of the total number of atoms in the entire sample at  $\Delta B = 30$  mG and  $V_L = 75 E_r$ . Solid curve shows the fitting to Eq. S5 to extract  $L_3$  with the squared atomic line density for the central tube  $n^2 = (N_{t,c}/2R_{F,c})^2$ . Data points are averaged over 5 shots, and the standard error of the mean is approximately equal to the symbol size.

We measure the time evolution with  $V_L$  between 15 to  $75 E_r$  and extract  $L_3$  by fitting to Eq. S5. The peak  $L_3$  as a function of  $V_L$  is shown in Fig. S3.

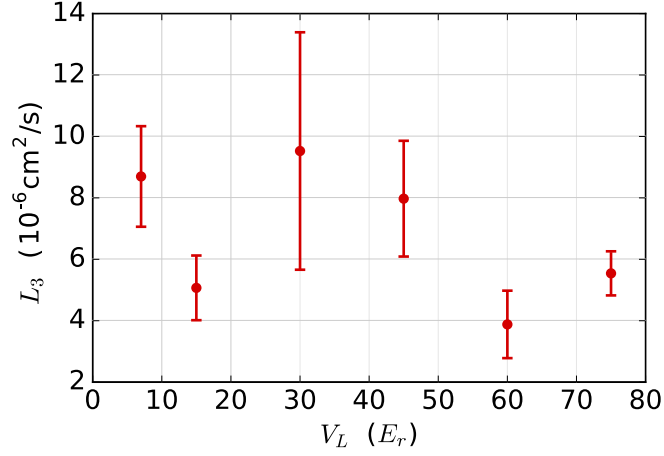


Figure S3. Peak three-body loss coefficient  $L_3$  as a function of lattice depth  $V_L$ .  $L_3$  is extracted by fitting the time evolution of  $N$  to Eq. S5 as described in the Fig. S2 caption. Error bars indicate the one-sigma confidence interval for the fitting parameters  $L_3$ .

### QUASI-1D $p$ -WAVE SCATTERING CROSS-SECTION

The quasi-1D  $p$ -wave scattering amplitude is [3]

$$f_{1D}(k) = \frac{-ik}{1/l_p + \xi_p k^2 + ik}, \quad (\text{S6})$$

In 1D, the equivalent of the scattering cross-section is simply the modulus of the scattering amplitude squared

$$\sigma_{1D}(k) = |f_{1D}(k)|^2 = \frac{k^2}{k^2 + (1/l_p + \xi_p k^2)^2}, \quad (\text{S7})$$

which is bounded from above by 1. Near a Feshbach resonance for  $l_p < 0$ , this expression may be approximated by a Lorentzian in terms of the collision energy,  $E = \hbar^2 k^2/m$  as follows:

$$\sigma_{1D}(E) \approx \frac{(\frac{\Gamma}{2})^2}{(E - E_{\text{res}})^2 + (\frac{\Gamma}{2})^2}. \quad (\text{S8})$$

Here,  $E_{\text{res}} = -\hbar^2/l_p \xi_p m > 0$  for  $l_p < 0$  is the above-threshold binding energy of the Feshbach molecule, and  $\Gamma = (\hbar/\xi_p)\sqrt{4E_{\text{res}}/m}$  is the width of the resonance [5].

### DEPENDENCE OF $\kappa a_{\perp}$ ON $V_L$

$\kappa$  is the magnitude of the wavevector related to the binding energy of the Feshbach molecule, which can be calculated by

$$\kappa = \frac{\sqrt{mE_{\text{res}}}}{\hbar} = \sqrt{\frac{-1}{l_p \xi_p}}. \quad (\text{S9})$$

where  $l_p$  and  $\xi_p$  are the 1D scattering parameters modified from 3D scattering quantities  $V_p$  and  $\alpha_p$  with confinement strength  $a_\perp$  as mentioned in the main text. By Taylor expanding  $\kappa^2$  around the Feshbach resonance field  $B_{1D}$  for a particular  $V_L$ , we find a constant  $\kappa$  at a fixed magnetic field detuning  $\Delta B$  which is independent of  $V_L$ :

$$\begin{aligned}\kappa^2(\Delta B) &= \kappa^2|_{B=B_{1D}} + \frac{\partial \kappa^2}{\partial B}|_{B=B_{1D}} \Delta B + \frac{\partial^2 \kappa^2}{\partial B^2}|_{B=B_{1D}} \Delta B^2 \\ &= \frac{\partial(1/V_p)}{\partial B}|_{B=B_{1D}} \Delta B + \frac{\partial^2(1/V_p)}{\partial B^2}|_{B=B_{1D}} \Delta B^2\end{aligned}\quad (\text{S10})$$

Therefore,  $\sqrt{2}\kappa a_\perp$  is proportional to  $V_L^{1/4}$  for a particular  $\Delta B$ , as shown in Fig. S4.

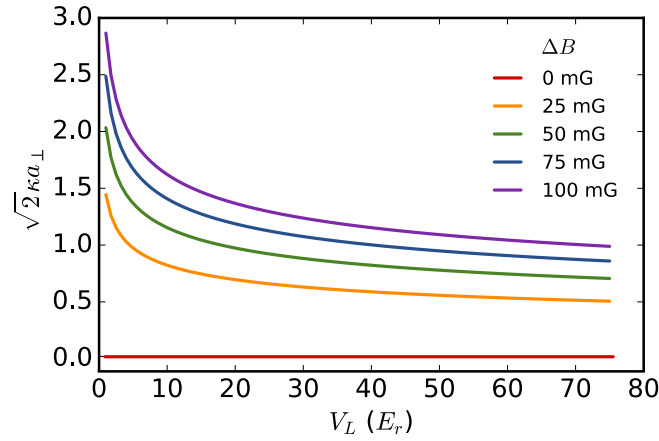


Figure S4.  $\sqrt{2}\kappa a_\perp$  as a function of lattice depth  $V_L$ . Each curve is  $V_L^{1/4}$  with a scaling factor set by  $\Delta B$ .

- 
- [1] B. E. Granger and D. Blume, Phys. Rev. Lett. **92**, 133202 (2004).
  - [2] L. Pricoupenko, Phys. Rev. Lett. **100**, 170404 (2008).
  - [3] D. V. Kurlov and G. V. Shlyapnikov, Phys. Rev. A **95**, 032710 (2017).
  - [4] M. Waseem, Z. Zhang, J. Yoshida, K. Hattori, T. Saito, and T. Mukaiyama, J. Phys. B **49**, 204001 (2016).
  - [5] V. Gurarie and L. Radzihovsky, Ann. Phys. (NY) **322**, 2 (2007).